11-2011

Optical Properties of Antiferroelectric Cs2Nb4O11: Absorption Spectra and First-Principles Calculations

H. L. Liu
National Taiwan Normal University

C. R. Huang
National Taiwan Normal University

G. F. Luo
University of Nebraska at Omaha

Wai-Ning Mei
University of Nebraska at Omaha, physmei@unomaha.edu

Optical properties of antiferroelectric $Cs_2Nb_4O_{11}$: Absorption spectra and first-principles calculations

H. L. Liu,[1,a)] C. R. Huang,[1] G. F. Luo,[2,b)] and W. N. Mei[2]
[1]*Department of Physics, National Taiwan Normal University, Taipei 11677, Taiwan*
[2]*Department of Physics, University of Nebraska at Omaha, Omaha, Nebraska 68182-0266, USA*

(Received 3 June 2011; accepted 22 October 2011; published online 28 November 2011)

We report a joint experimental and theoretical investigation of the optical properties of $Cs_2Nb_4O_{11}$. In room temperature optical absorption spectra, we found a direct gap about 3.55 ± 0.05 eV and charge transfer excitations at about 4.96 and 6.08 eV, which are in good agreement with the first-principles calculations. Upon passing through the 165 °C antiferroelectric to paraelectric phase transition, the peak energies of two charge transfer bands display almost no temperature dependence, yet they become even broader and exhibit enhanced oscillator strength. We infer this intriguing behavior as the manifestation of Nb cation distortions due to the charge-lattice interaction. © *2011 American Institute of Physics*. [doi:10.1063/1.3663341]

I. INTRODUCTION

Solid-state antiferroelectrics are promising materials for multiple-state memory applications,[1] mainly because they are analogous to antiferromagnetic materials, in which each individual electric dipole is antiparallel to that of the nearest neighbors; thus, the net polarization of the entire structure is zero. Under the action of an external electric field, they would show three polarization states: up, down, and off, depending on the strength and direction of the applied field. One system with an orthorhombic structure that has attracted attention in this regard is $Cs_2Nb_4O_{11}$, as shown in Fig. 1. As we notice, it consists of NbO_6 octahedra and NbO_4 tetrahedra connected through shared vertices and edges, with Cs atoms occupying channels provided by the three-dimensional polyhedral network.[2] In recent reports, $Cs_2Nb_4O_{11}$ is demonstrated to be an antiferroelectric based on the double hysteresis loops in electric field versus polarization plot.[3] Moreover, it transforms at 165 °C from a low-temperature antiferroelectric phase in space group *Pnna* to a high-temperature paraelectric phase in space group *Imma*.[4,5] In addition, $Cs_2Nb_4O_{11}$, particularly when doped with oxides, $Cs_2Nb_4O_{11}$ is known to be an effective photocatalyst for its special ability in decomposing water into hydrogen and oxygen gases,[6] hence, rendering optical properties of $Cs_2Nb_4O_{11}$ attractive, however, have remained largely unexplored.

In fact, a theoretical study was reported not long ago that the bandgap of $Cs_2Nb_4O_{11}$ is direct and about 3.1-3.2 eV;[5] also, the calculated band structure was found to be conducive to its observed photocatalytic properties. In order to further elucidate the optical properties of $Cs_2Nb_4O_{11}$, we employed two effective techniques, the optical reflectance spectroscopy and spectroscopic ellipsometry, so that we can first determine essential optical properties such as optical conductivity and dielectric function, then deduce major electronic features and optical transitions. Hence, corroborating with the first-principles computation, we are able to deduce an in-depth description for the optical properties of the material.

II. TECHNICAL DETAILS

A. Experiment

Single crystals of $Cs_2Nb_4O_{11}$ were grown from the binary system using the flux method. A detailed description of the sample preparation can be found elsewhere.[7] Typical crystal dimensions were $\sim 2 \times 2 \times 1$ mm^3. The crystals were cleaved to yield a shiny surface corresponding to the *ac* plane. Characterizations of x ray diffraction and electric field dependence of polarization have also been performed on similar samples.[3,5]

Near-normal infrared and optical reflectance measurements were carried out at room temperature. A Bruker IFS 66v Fourier transform infrared spectrometer was used in the far- infrared and mid-infrared regions (30–6000 cm^{-1}), while the near-infrared to near-ultraviolet regions (4000–55000 cm^{-1}) were covered using a Perkin-Elmer Lambda-900 spectrometer. Spectral resolution is 2 cm^{-1}. The optical properties (i.e., the complex conductivity $\sigma(\omega) = \sigma_1(\omega) + i\sigma_2(\omega)$ or dielectric function $\varepsilon(\omega) = 1 + 4\pi i\sigma(\omega)/\omega$ were calculated from a Kramers-Kronig analysis of the reflectance data.[8] To perform these transformations, one needs to extrapolate the reflectance at both low and high frequencies. At low frequencies, the extension was done by modeling the reflectance using the Lorentz model and using the fitted results to extend the reflectance below the lowest frequency measured in the experiment. The high-frequency extrapolations were done by using weak power law dependence, $R \approx \omega^{-s}$ with $s \approx 1$–2.

Ellipsometric spectra were collected under multiple angles of incidence between 60° and 75° using a Woollam M-2000 rotating compensator multichannel spectroscopic ellipsometer over a spectral range from 0.73 to 6.42 eV. For high temperature measurements, the ellipsometer was

a)Author to whom correspondence should be addressed. Electronic mail: hliu@phy.ntnu.edu.tw.
b)Current address: Department of Theoretical and Computational Molecular Science, Institute for Molecular Science, Okazaki 444-8585, Japan.

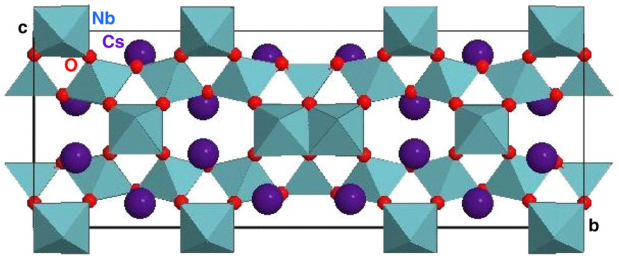

FIG. 1. (Color online) Room temperature $Cs_2Nb_4O_{11}$ structure view along the *a*-axis.

equipped with a vacuum hot stage system. Due to the 70° angle of the two stage windows, only a single angle of incidence is possible. The raw ellipsometry data Ψ and Δ are related to the complex Fresnel reflection coefficients for light polarized parallel (R_p) and perpendicular (R_s) to the plane of incidence

$$e^{i\Delta}\tan\Psi = \frac{R_p}{R_s}. \quad (1)$$

To determine the complex dielectric response of $Cs_2Nb_4O_{11}$, the experimental data were processed using the model of an air-homogeneous isotropic substrate. Then, the error function σ was minimized in the entire spectral range:

$$\sigma^2 = \frac{1}{m}\sum_{i=1}^{m}\left[\left(\Delta_{exp}-\Delta_{calc}\right)^2+\left(\Psi_{exp}-\Psi_{calc}\right)^2\right], \quad (2)$$

where Δ_{calc}, Ψ_{calc} and Δ_{exp}, Ψ_{exp} are, respectively, the calculated and experimental ellipsometric data and m is the number of points in the spectrum. The Lorentz approximation was used to fit the spectral dependence of Ψ and Δ and calculate the dielectric function.

B. Theoretical methods

Our calculations were carried out in the framework of density-functional theory[9] within the local density approximation (LDA),[10] as implemented in the CASTEP code.[11] The geometrical structures are fully optimized until the maximum force on each atom is less than 3×10^{-2} eV/Å and the stress less than 5×10^{-2} GPa. The plane wave energy cutoff is 340 eV together with ultrasoft pseudopotentials. In Brillouin zone sampling, the *k*-point sampling spacing is ~0.04 $Å^{-1}$ in the ground state calculations and ~0.009 $Å^{-1}$ in the optical spectrum calculations. The imaginary part of the dielectric function ε_2 is given by the Fermi's golden rule expression:[12]

$$\varepsilon_2(\omega) = \frac{1}{4\pi\varepsilon_0}\left(\frac{2\pi e}{m\omega}\right)^2\sum_{k,c,v}|\langle\psi_k{}^c|e\cdot p|\psi_k{}^v\rangle|^2\delta(E_k{}^c-E_k{}^v-\hbar\omega), \quad (3)$$

where e is the polarization vector of the incident electric field, p is the momentum operator, and *c* and *v* represent the conduction and valence bands, respectively.

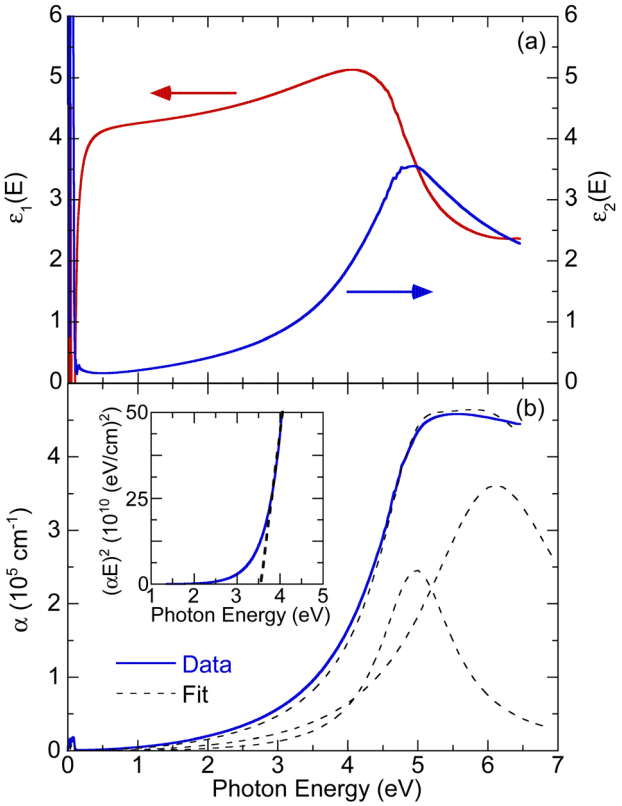

FIG. 2. (Color online) (a) Room temperature dielectric function spectra obtained from analysis of optical reflectance spectrum of $Cs_2Nb_4O_{11}$. Curves with arrows pointing to the left and right are the real and imaginary parts, respectively. (b) Optical absorption coefficient of $Cs_2Nb_4O_{11}$ at 300 K. The two fitted Lorentz oscillators in black dashed lines are also shown. In the inset, we show the deduction of the $Cs_2Nb_4O_{11}$ direct bandgap.

III. RESULTS AND DISCUSSION

In Fig. 2(a), we show the room-temperature real ε_1 and imaginary ε_2 parts of the dielectric function $\varepsilon(E)$ calculated by using the Kramers-Kronig analysis on the optical reflectance curves. We notice that the dispersive response in ε_1 exhibits typical behavior of a semiconductor,[13] with an overall positive value, except for the far-infrared regions with strong phonon dispersions. Optical transitions can be identified in the spectra by resonance and antiresonance features that appear at the same energy in ε_2 and ε_1, respectively. Notably, the spectrum ε_2 is dominated by two broad optical transitions, with detailed analysis shown below. In Fig. 2(b), we display the optical absorption spectrum determined from spectroscopic ellipsometry analysis, which is complementary to that obtained from optical reflectance. As we can see beyond the region of 0.1 eV, usually characterized as phonon response, the absorption gradually increases, manifests a sharp rise from 3.0 eV, reaches a maximum value about 5.0 eV, and then levels off. In a normal solid, one expects that the absorption coefficient, $\alpha(E)$, consists of contributions from both the direct and indirect bandgap transitions[14] and is given by

$$\alpha(E) = \frac{A}{E}\left(E-E_{g,dir}\right)^{0.5}+\frac{B}{E}\left(E-E_{g,ind}\mp E_{ph}\right)^2, \quad (4)$$

where $E_{g,dir}$ and $E_{g,ind}$ are the magnitudes of direct and indirect gaps, respectively, E_{ph} is the emitted (absorbed) phonon

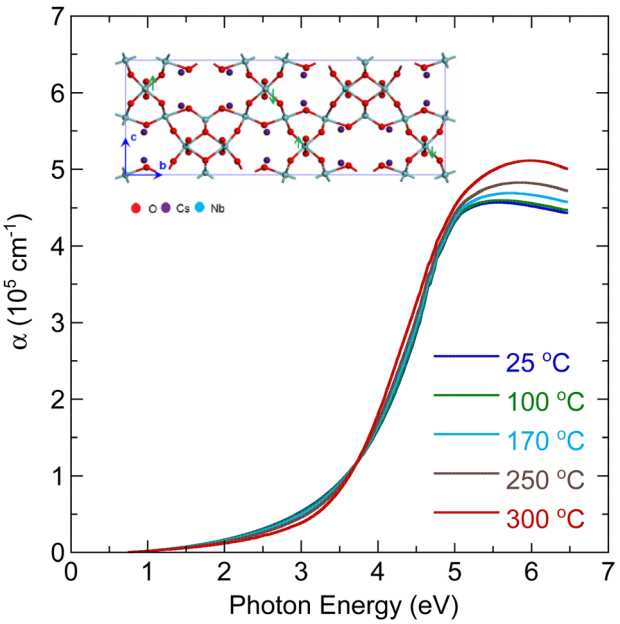

FIG. 3. (Color online) Temperature dependence of optical absorption coefficient of $Cs_2Nb_4O_{11}$ obtained from spectroscopic ellipsometry analysis. In the inset, we show the distortions of the NbO_6 octahedra in a low-temperature antiferroelectric phase.

energy, and A and B are constants. This model, while assuming a simple band shape, allows for extraction of the direct energy gap by plotting $(\alpha \cdot E)^2$ as a function of photon energy. Linear extrapolation of $(\alpha \cdot E)^2$ to zero yield a gap of 3.55 ± 0.05 eV, as shown in the inset of Fig. 2(b). Plotting $(\alpha \cdot E)^{0.5}$ as a function of photon energy led to an unsatisfactory fit, with no evidence of photons being emitted/absorbed, implying that $Cs_2Nb_4O_{11}$ is a direct gap material. Two optical excitations near 4.96 and 6.08 eV are assigned as electron band transitions of the O 2*p* and Nb 4*d* states based on the partial density of states analyses decomposed to three different composite elements of $Cs_2Nb_4O_{11}$.[5]

In Fig. 3, we show the temperature dependence of optical absorption spectra extracted from our ellipsometric data. There are several important features to these spectra. First, when the sample is heated from 25 °C to 100 °C, we do not observe any sharp changes in absorption, but rather a continuous gradual growth, i.e., the absorption at the highest energy increases only about 1% of that at the lowest energy. Second, above 165 °C, we see a suppression of the low-energy absorption below 3.5 eV and there is an increase in absorption in the energy range between 5.0 and 6.4 eV, indicating that important changes occur in the electronic structures as a result of the antiferroelectric to paraelectric phase

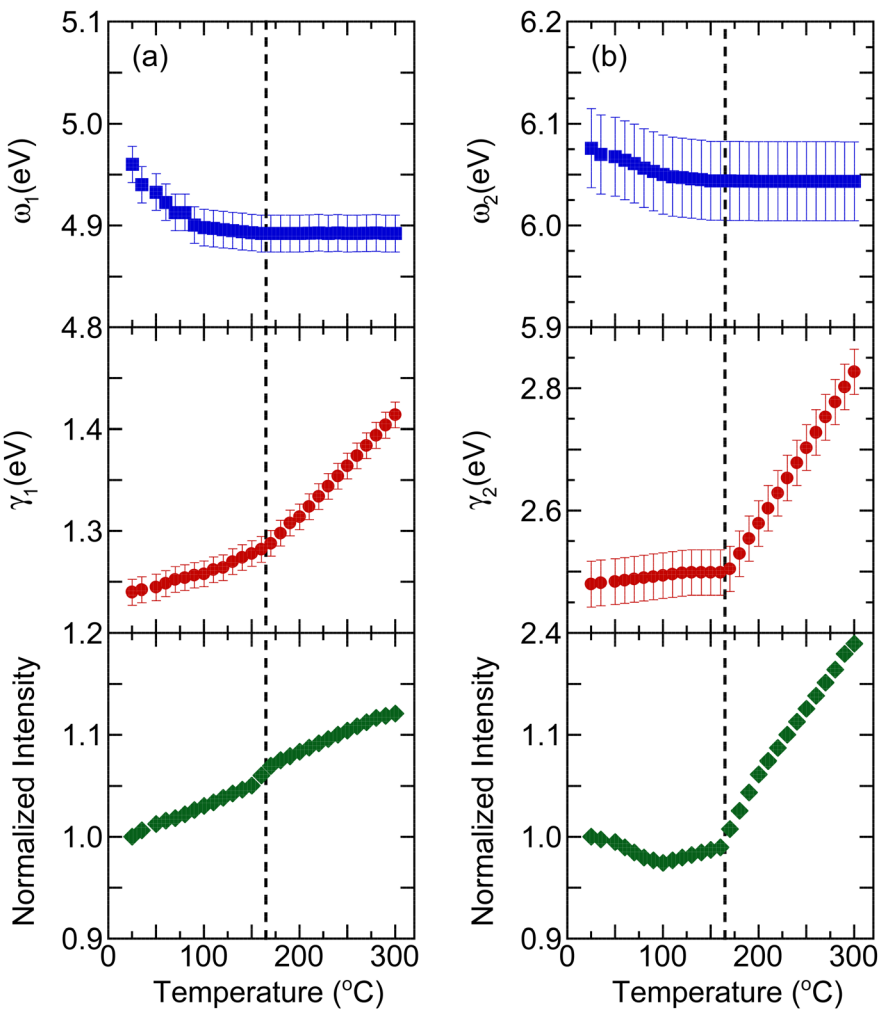

FIG. 4. (Color online) Temperature dependence of peak energy, damping, and normalized intensity of two optical absorption transitions in $Cs_2Nb_4O_{11}$. Dotted vertical lines indicate the 165 °C antiferroelectric to paraelectric phase transition temperature.

transition. Third, we find the bandgap exhibits very weak temperature dependence, i.e., the value of 300 °C direct bandgap is about 3.50 ± 0.05 eV.

To illustrate the temperature-dependent changes of the optical absorption spectra, we fit our data using a classical Lorentzian model for the complex dielectric function[8]

$$\varepsilon(\omega) = \sum_{j=1}^{N} \frac{\omega_{pj}^2}{\omega_j^2 - \omega^2 - i\omega\gamma_j} + \varepsilon_\infty, \quad (5)$$

where ω_j, γ_j, and ω_{pj} are the frequency, damping, and oscillator strength of the jth Lorentzian contribution and ε_∞ is the high frequency limit of $\varepsilon(\omega)$, which includes interband transitions at frequencies above the presently measured range. Then, the absorption coefficient is simply given as $\alpha(\omega) = \frac{2\omega}{c}\sqrt{\frac{1}{2}\left[\sqrt{\varepsilon_1(\omega)^2 + \varepsilon_2(\omega)^2} - \varepsilon_1(\omega)\right]}$. Afterward, in Fig. 4, we show the peak energy, damping, and normalized intensity of two optical transitions as a function of temperature. It becomes clear that two optical absorptions associated with charge transfer excitations shift to lower energies and their dampings increase with increasing temperature until 165 °C. In fact, the discontinuous changes in the damping and absorption manifest the phase change and phonon participation before and after the transition. As for the early drops of the optical transition frequencies, we regard that this might be caused by the micro-domains in the samples, i.e., the transition temperatures in the domain are usually lower than the bulk value. Notably, above 165 °C, the peak energies of two charge transfer transitions display almost no temperature dependence, yet they become even broader and exhibit enhanced spectral weight. According to our previous first-principles calculations,[5] the antiferroelectricity in $Cs_2Nb_4O_{11}$ originates from the distortions of the NbO_6 octahedra and the displacements of the niobium atoms contained therein. Therefore, we attribute the observed phenomena in charge-transfer excitations at 165 °C, mainly due to the local structure distortions in the NbO_6 octahedra of $Cs_2Nb_4O_{11}$.

In order to acquire deeper understanding on the temperature-dependent mechanism in optical absorption of $Cs_2Nb_4O_{11}$, we performed first-principles calculations based on the determined geometric structure in our previous studies.[5] In Fig. 5, we present the optical absorption spectra of the low-temperature (LT) and high-temperature (HT) phases of $Cs_2Nb_4O_{11}$ with unpolarized incident light. We notice that, in the range of 0–10 eV, there are two dominant peaks: the highest one around 4.7 eV and the second highest one around 6.1 eV. Specifically, the peak around 4.7 eV is 0.03 eV lower in the HT phase than that in the LT phase, as is generally consistent with the ~0.05 eV redshift in the experiment (Fig. 5(a)). The peak around 6.1 eV is almost the same in both phases.

In Fig. 6, we show the partial density of states (PDOS) analyses; notice that the conduction band states originating from the Nb 4*d* electrons shift to low energy in HT phase with their valence band states almost remaining unchanged. Hence, the corresponding optical absorption peak should demonstrate downward changes in HT phase, and the Nb 4*d*

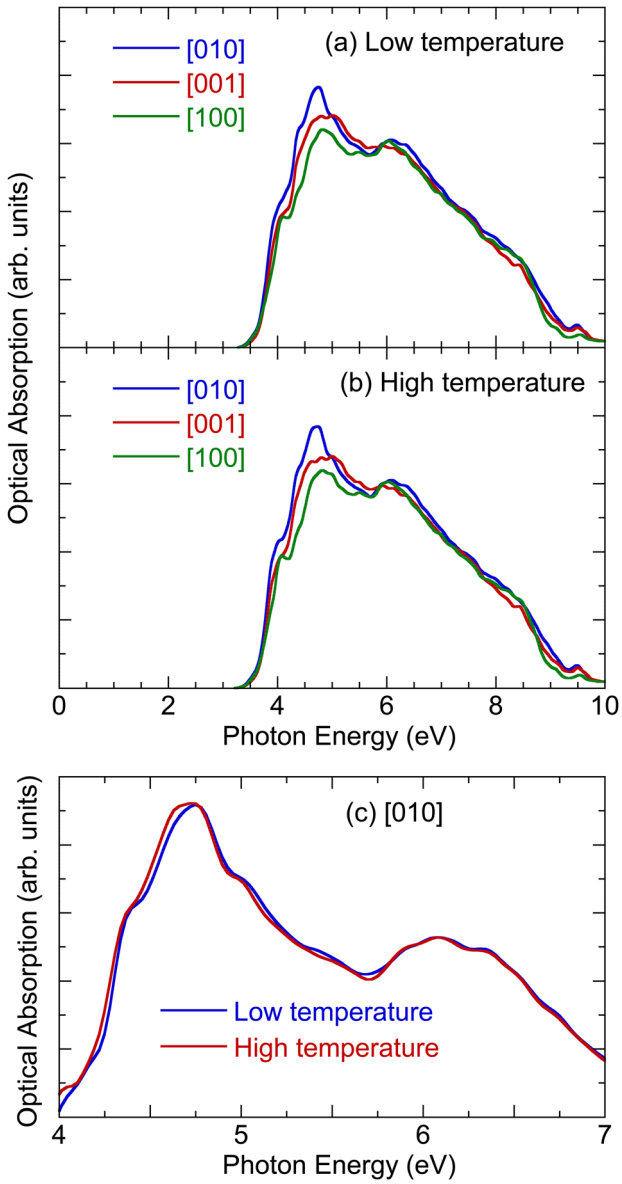

FIG. 5. (Color online) Calculated optical absorption spectra of the (a) LT and (b) HT phases $Cs_2Nb_4O_{11}$ with unpolarized light propagating along the [010], [001], and [100] direction. Spectrum comparison between LT and HT phases are shown in (c) for the [010] direction.

electron transitions could be the major cause of the peak around 4.7 eV. Also, we observe that both the conduction and valence band mainly coming from the O 2*p* electrons red-shift in the HT phase; consequently, the optical absorption peak shows no obvious change and, thus, the peak around 6.1 eV could be contributed solely from the O 2*p* electron transitions.

From spectra in Fig. 5(c), we also observe that that the HT phase possesses slightly higher intensity in the region of 3–5 eV, which is consistent with peak intensity variation in our experiment, shown in Fig. 4(a). Actually, such change can be traced back to the partial density of states shown in Fig. 6: since the conduction band states of the *d* electrons are higher in the HT phase, the joint density of states and optical absorption intensity follow the similar trend. As for the spectra in the region of 5.5–7 eV, the intensities are almost the

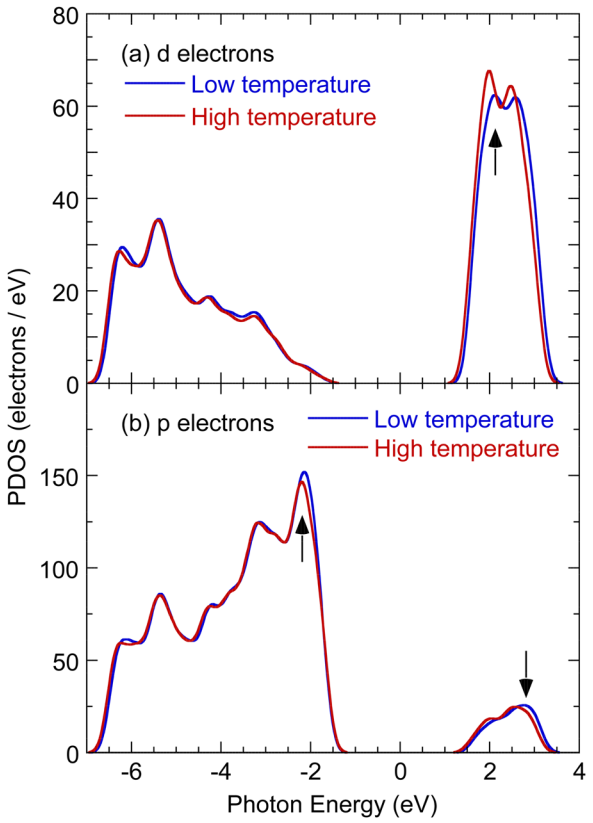

FIG. 6. (Color online) Partial density of states of the (a) *d* and (b) *p* electrons, which mainly come from the Nb 4*d* and O 2*p* in the shown energy region. Fermi energy level is set to zero, and arrows indicate the positions of the major differences between the two phases.

same in both phases: we explain them in terms of the slight partial density changes of *p* electrons between the two phases.

IV. SUMMARY

We employed both optical reflectance spectroscopy and spectroscopic ellipsometry to elucidate the optical properties of $Cs_2Nb_4O_{11}$ and compared our results with the predictions of first-principles calculations. At room temperature, the material has a direct bandgap of 3.55 ± 0.05 eV. The optical absorption spectra exhibit two features centered at about 4.96 and 6.08 eV that we assign as charge transfer transitions between the O 2*p* and Nb 4*d* states. These results are in good agreement with those obtained from the first-principles calculations. With increasing temperature, the peak energy, damping, and oscillator strength of these two absorption bands behave anomalously above the 165 °C antiferroelectric to paraelectric phase transition temperature. Based on our findings, we suggest that as a result of the local lattice rearrangement of niobium during phase transition, the coordination shifts in NbO_6 octahedra cause the $Cs_2Nb_4O_{11}$ electronic structure to readjust.

ACKNOWLEDGMENTS

H.L.L. would like to acknowledge financial support from the National Science Council of Republic of China under Grant No. NSC 98-2112-M-003-004-MY3. G.F.L. is supported by the Specially Promoted Research from the MEXT in Japan, and W.N.M. would like to thank the support from the Nebraska Research Initiative and DOE DE-EE0003174 in the United States and helpful discussions from R. Smith and R. F. Sabrianov.

[1]E. Buixaderas, S. Kamba, and J. Petzeit, Ferroelectrics **308**, 131 (2004).
[2]P. M. Gasperin, Acta Crystallogr. **B37**, 641 (1981).
[3]R. W. Smith, C. Hu, J. Liu, W. N. Mei, and K. J. Lin, J. Solid State Chem. **180**, 1193 (2007).
[4]J. Liu, E. P. Kharitonova, C.-G. Duan, W. N. Mei, R. W. Smith, and J. R. Hardy, J. Chem. Phys. **122**, 144503 (2005).
[5]R. W. Smith, G. Luo, and W. N. Mei, J. Phys. Chem. Solids **71**, 1357 (2010).
[6]Y. Miseki, H. Kato, and A. Kudo, Chem. Lett. **34**, 54 (2005).
[7]E. P. Kharitonova, V. I. Voronkova, V. K. Yanovskii, and S. Y. Stefanovich, J. Cryst. Growth **237-239**, 703 (2002).
[8]F. Wooten, *Optical Properties of Solids* (Academic, New York, 1972).
[9]P. Hohenberg and W. Kohn, Phys. Rev. **136**, B864 (1964).
[10]W. Kohn and L. J. Sham, Phys. Rev. **140**, A1133 (1965).
[11]M. D. Segall, P. J. D. Lindan, M. J. Probert, C. J. Pickard, P. J. Hasnip, S. J. Clark, and M. C. Payne, J. Phys.: Condens. Matter **14**, 2717 (2002).
[12]P. Y. Yu and M. Cardona, *Fundamentals of Semiconductors: Physics and Materials Properties*, 3rd ed. (Springer, New York, 2001).
[13]P. Gori, M. Rakel, C. Cobet, W. Richter, N. Esser, A. Hoffmann, R. D. Sole, A. Cricenti, and O. Pulci, Phys. Rev. B **81**, 125207 (2010).
[14]J. I. Pankove, *Optical Processes in Semiconductors* (Dover, New York, 1971).